Spectroscopic Study of the Thermal Degradation of PVP-capped Rh and Pt Nanoparticles in H_2 and O_2 environments

Yuri Borodko,[a] Hyun Sook Lee,[a] Sang Hoon Joo,[b] Yawen Zhang,[b] and Gabor Somorjai [a,b,*]

a) Chemical and Materials Sciences Divisions, Lawrence Berkeley National Laboratory, 1 Cyclotron Road, Berkeley CA 94720
b) Department of Chemistry, University of California, Berkeley, CA 94720

Abstract

Poly(N-vinylpyrrolidone (PVP) capped platinum and rhodium nanoparticles (7 - 12 nm) have been studied with UV-VIS, FTIR and Raman spectroscopy. The absorption bands in the region 190 – 900 nm are shown to be sensitive to the electronic structure of surface Rh and Pt atoms as well as to the aggregation of the nanoparticles.

In-situ FTIR-DRIFT spectroscopy of the thermal decay of PVP stabilized Rh and Pt nanoparticles in H_2 and O_2 atmospheres in temperatures ranging from 30 ^oC – 350 ^oC reveal that decomposition of PVP above 200 ^oC, PVP transforms into a 'polyamid-polyene' - like material that is in turn converted into a thin layer of amorphous carbon above 300 ^oC. Adsorbed carbon monoxide was used as a probing molecule to monitor changes of electronic structure of surface Rh and Pt atoms and accessible surface area. The behavior of surface Rh and Pt atoms with ligated CO and amide groups of pyrrolidones resemble that of surface coordination compounds.

Introduction

Poly(vinylpyrrolidone) (PVP) is used extensively as a flexible membrane for stabilizing metallic nanocrystals with varying size and shape [1]. The application of Pt-PVP and Rh-PVP nanoparticles in catalytic reactions has recently offered promising new opportunities to create tailored catalytic systems [2]. The knowledge of the structure and properties of the interface between the capping agent and the metal surface is critical for understanding nanoparticles role in catalytic reactions, since capping agents can stabilize specific

electronic states of the surface atoms, thus creating specific catalytic active sites. A routine procedure used to activate heterogeneous catalysts is redox cycling treatment of the catalysts at elevated temperatures. This may induce changes in the electronic structure of metallic atoms, the size and shape of the nanoparticles, the chemical state of the capping agent, and in the area of metallic surface that is accessible to the reactants. To minimize temperature effects and retain the shape and size of Pt-PVP and Rh-PVP nanoparticles, temperatures usually do not exceed 100º-300 ºC. However, in this temperature range capping agents can be decomposed, especially in reactive media such as O_2 and H_2. It should be noted, that treatment of organic stabilizer in ozone-reach atmosphere is promising option for removing the capping agent at low temperature [2a]. In this paper, we report a study of the structure and stability of pure PVP and PVP-capped Rh and Pt nanoparticles using *in-situ* spectroscopic measurements. UV-VIS spectra reveal that the charge-transfer (CT) band (330 nm) and optical surface plasma-resonance absorption (245 nm), are surface sensitive. The intensity of the CT band shows sensitivity towards the electronic structure of Pt and Rh atoms on the surface as well as the aggregation of the nanoparticles, whereas optical plasmon band appears only for aggregated nanoparticles. FTIR-DRIFT studies as a function of temperature found that the decay of the inner PVP capping layer, which is bonded to the surface metal atoms, begins ~100 ºC lower than the decay of the outer unbound PVP capping layer or of pure PVP. Carbon monoxide chemisorbed on the surface of metal nanoparticles shows subtle IR changes that are a result of donor-acceptor interactions between polymer amide groups and surface metal atoms. Formation of some intermediates that form during the degradation of capping PVP on Pt and Rh as the temperature is increased was detected in

the IR with characteristic bands: NH (3342 cm^{-1}), CH (3089 cm^{-1}), C≡N (2246 cm^{-1}) and C=C-C=C (1595 cm^{-1}). Further heating of Rh- and Pt-PVP above 300 ºC leads to the formation of a thin layer of a complex composite: 'polyamide-polyene' like fragments together with amorphous carbon.

Experimental Section

Chemicals. Rhodium (III) acetylacetonate ($Rh(acac)_3$, 97%), Platinum (II) acetylacetonate ($Pt(acac)_2$, 97%), 1,4-butandiol(99%), poly(vinylpyrrolidone) (PVP, Mw=55K), and acetylacetone (Hacca, 99%) were purchased from Aldrich and used as received. All solvents (acetone, ethanol, hexane and chloroform) were analytical grade and used without further purification.

Synthesis of Pt and Rh nanoparticles. For synthesis of PVP capped Rh nanoparticles we use 0.25 mmol $Rh(acac)_3$ with 2.5 mmol of PVP dissolved in 20 ml of 1,4-butanediol [3]. The stock solution was heated to 140 ºC in a Glass-Col electromantle (60W; 50ml) and was evacuated at this temperature for 20min to remove water and oxygen under magnetic stirring, resulting in an optically transparent orange-yellow solution. The flask was then heated to the desired reaction temperature, between 170 and 230 ^oC, at a rate of 10 $^oC\ min^{-1}$, and maintained at this temperature (±2 ^oC) for 2 hours under an Ar atmosphere. During the reaction, the color of the solution gradually turned from orange-yellow to black. When the reaction was complete, an excess of acetone was poured into the solution at room temperature to form a cloudy black suspension. This suspension was separated by centrifugation at 4200 rpm for 6 min, and the black product was collected by discarding the colorless supernatant. The precipitated Rh nanoparticles were washed with acetone once and then redispersed in ethanol in three-necked flask at

room temperature. Platinum nanoparticles were prepared by using the same method, but instead using 0.1 mmol $Pt(acac)_2$ with 1 mmol PVP dissolved in 20 ml of 1,4-butanediol as starting materials. **TEM** analysis of the Rh or Pt nanoparticles analysis was carried out with a Philips FEI Tecnai 12 transmission electron microscope operated at 100 kV. The average size of Pt nanoparticles was 12 ± 3 nm and 8 ± 2 nm for Rh nanoparticles (Figure 1).

Spectroscopic Characterization

UV-VIS. Optical properties of Pt and Rh nanoparticles were characterized using a UV-VIS spectrophotometer, Perkin-Elmer, LAMDA 650 (190 nm-900 nm). Spectra were taken of drop casted films deposited on a quartz window in transmission or Al-foil in reflectance with an integrating sphere of 60 mm in diameter coated with spectralon . The morphology of Rh- and Pt-PVP nanoparticles deposited on Si-wafers was characterized with **SEM** using a Zeiss Gemini Ultra-55 analytical scanning electron microscope, before and after heating in air.

FTIR-DRIFT spectra were measured with a Nicolet Nexus-670 spectrophotometer with integrated diffuse reflectance optics (Spectra-Tech Collector II). The improved spectra could be obtained by using a thin layer of PVP/Pt or PVP/Rh deposited on aluminum foil. Since the layer thickness can be adjusted so as to render the sample partially IR transparent, we were able to optimize the ratio of diffuse to specular reflectance and obtain spectra of similar quality compared to those measured in transmission mode [4]. The temperature/vacuum chamber Spectra-Tech 0030-101 was used for *in-situ* FTIR measurements in 5% H_2 balanced with N_2 and pure O_2 flow, or a static CO atmosphere. An oil-free Alcatel Drytel 34 turbo-pump station was used for sample evacuation.

The deep UV-Raman spectroscopy system was described in detail elsewhere [5, 6]. A continuous wave (cw) intracavity double argon ion laser operating at 244 nm is used as the excitation source. Backscattered light was collected and directed to the triple spectrometer Spex 1877C, which was optimized for performance in the deep UV region. Spectra were recorded with an LN_2-cooled, UV-enhanced CCD camera. The instrument dispersion is 2.1 cm^{-1}/pixel; the typical resolution was 12 cm^{-1}.

To eliminate decomposition of Pt and Rh-PVP samples under UV irradiation we used a custom designed rotating sample holder (400-1200 rpm) equipped with a second motor for lateral translation (240 rpm). In this manner, the laser beam was XY-rastered over the entire sample (deposited on Al-foil) decreasing the UV exposure in a given spot by 10^{-3} when compared with a static sample holder. Typical collection times were 5-30 min, using 3-5 mW of 244 nm excitation energy. GRAMS/AI and Omnic software from Thermo Galactic was used for processing FTIR-DRIFT and UV-Raman spectra.

X-ray diffraction patterns were measured on a Bruker D8 GADDS diffractometer using Co Kα radiation (1.79 Å). XRD samples were prepared by depositing the nanoparticles on a glass plate. Different chemically-inert supporting materials were used for characterization of the metal nanoparticles: quartz windows for UV-VIS transmission; Al-foils for UV-VIS reflection and FTIR-DRIFT; glass plates for XRD and Si-wafers for SEM.

RESULTS and DISCUSSION

UV-VIS spectra of Rh-PVP and Pt-PVP

Recently, UV-VIS absorbance spectra for Rh-PVP nanoparticles in solution have been presented in [7]. We have taken the UV-VIS spectra of PVP, Rh-PVP, and Pt-PVP as: i)

absorbance of a homogeneous solution, ii) absorbance of a drop-cast film deposited on a quartz window, and iii) reflectance of a film deposited on aluminum foil in the region of 200-900 nm. The UV-VIS spectrum of PVP has a narrow intense band at 200 nm, which may be assigned to $n \rightarrow \pi^*$ transitions between the oxygen lone pairs and the vacant π^*-orbital of the pyrrolidone ring (Fig. 2A). The absorbance spectra of PVP are very similar for cases i and ii. In the spectra of Rh-PVP and Pt-PVP, along with the $n \rightarrow \pi^*$ band at 200 nm, new bands appear near 330 nm and 300 nm respectively, which may be assigned to charge-transfer transitions of an electron excited from the carbonyl lone pair to a vacant d-orbital of the metallic nanoparticles (Fig. 2B). Thus, the spectra of Rh-PVP and Pt-PVP nanoparticles in the UV region have two bands, one being characteristic of a loose shell of the polymeric stabilizer around a metallic core and the other of a single surface layer formed between chemisorbed carbonyl groups and surface metallic atoms $>C=O \rightarrow Rh^{\delta+}$ or $Pt^{\delta+}$. This interpretation of UV absorption spectra of Rh-PVP and Pt-PVP is in good agreement with our recent observations of CT-SERS effects for these nanoparticles by deep UV Raman [5, 6]. It was found that the UV-VIS spectra of nanoparticles differ substantially depending on the sample aggregation. The aggregation causes multiple scattering and changes the spectra depending on the mode of measurement (transmission or reflection) [8]. As seen in Figures 2B and 2C, the ratio of $n \rightarrow \pi^*$ band to that of the CT band for a homogeneous EtOH solution is higher in transmission than for a drop-cast film deposited on Al-foil in reflection. This is a result of multiple scattering of light on aggregated Rh-PVP nanoparticles. The thicker the layer of Rh-PVP on Al foil, the stronger is the CT band at 330 nm relative to the intensity of the $n \rightarrow \pi^*$ band at 200 nm (Figure 2C). The contribution of multiple reflections from the

surface of metallic nanoparticles in thick films increases due to the aggregation of nanoparticles, leading to substantial increases in CT band intensity. The thickness of drop-cast layers was estimated from the Fabry-Perot fringe separation that arise from the interference between beams transmitted and partially reflected at the film-quartz interface shown in the insert in Figure 2D. The effective thickness of drop-cast films under study was in the range 1.5-5μm , calculated using the expression $d = \Delta m/[2(n^2 - Sin^2\Theta)^{1/2}\Delta v_{if}]$, where Δm is the number of fringes, Δv_{if} is the wavenumber difference between the initial and final fringe, and Θ is the angle of incidence [9]. The value of the refractive index n for Pt-PVP and Rh-PVP layers was taken as 1.5.

Influence of temperature on UV-VIS spectra. Rh and Pt metallic nanoparticles stabilized by PVP are characterized by four types of absorption bands in the UV-VIS region (Figure 3). Three types of electronic transition are inherently characteristic of nanoparticles when the size is less than the mean free path of electrons. The additional band for optical plasma-resonance absorption should develop as a result of aggregation of metallic nanoparticles when the aggregate size is above 20-30 nm. UV-VIS reflection spectra of Pt and Rh nanoparticles subjected to reduction in hydrogen flow at temperatures ranging from 30°-170°C show a weak dependence on the temperature (Figure 3A). At 170°C the intensity of charge-transfer bands slightly decreased due to reduction of Pt/Rh atoms on the surface of nanoparticles, since the interaction of a carbonyl group of PVP and Pt/Rh atoms on oxidized metal nanoparticle surfaces is stronger than on the reduced surfaces [5, 6]. UV-VIS spectra were also studied for drop-casted samples deposited on a quartz window and subjected to heating in air in the temperature range 20°-550°C. Recently it was shown that during the oxidation of Rh

nanoparticles in air at elevated temperatures, both the decomposition of the PVP layer and the oxidation of rhodium atoms on the surface to form a RhOx layer occur [10]. Pt nanoparticles (with diameters > 3 nm) are more stable towards oxidation and produce only a single oxide layer of PtOx [11]. As can be seen in Figure 3B, after treatment in air at elevated temperatures, the band at 200 nm ($n \rightarrow \pi^*$ for loosely bonded pyrrolidone rings) and CT bands at 330 nm disappear and new bands at 227 nm, 370 nm, and 590 nm gradually appear. This transformation of UV spectrum suggests decomposition of the capping PVP and aggregation of metallic nanoparticles. With this possibility in mind, the X-ray diffraction for nanoparticles heated in air was studied.

The XRD diffraction patterns of Pt and Rh nanoparticles are shown in Fig 4 for samples heated in air at 50 °C, 250 °C, and 450 °C for 15 min. The three peaks correspond to Bragg reflections of the (111), (200), and (220) crystal planes of the metallic core of Pt and Rh nanoparticles. The inserts in Figures 4A and 4B reveal that the (111) reflection becomes sharper after heating at higher temperatures. The mean diameter of the nanoparticles (calculated by the Debye-Scherrer formula) increases about 20% and 35% for Pt and Rh, respectively, after heating to 450 °C (Table 1).

TABLE 1

SAMPLE	FWHM	Θ	d(nm)
Pt/PVP_50 °C	1.02	23.32	9.7
Pt/PVP_250 °C	0.92	23.32	10.8
Pt/PVP_450 °C	0.85	23.27	11.7
Rh/PVP_50 °C	1.83	24.00	5.5
Rh/PVP_250 °C	1.85	24.00	5.4
Rh/PVP_450 °C	1.35	24.06	7.4

SEM images show that the morphology of Rh-PVP and Pt-PVP drop-cast films deposited on Si wafers changes substantially after heating. At temperatures above 400 °C, the 9.7 nm Pt and 5.5 nm Rh nanoparticles form 50-80 nm aggregates (Figure 4). To gain insight into how aggregation changes the optical properties of the nanoparticles, backward scattered light of Rh-PVP deposited on a quartz window was measured using an integrating sphere. In this experimental configuration, the sample is placed on the port of the integrating sphere and a black absorber behind the sample is used to minimize the contribution of specular reflection and transmitted light (Figure 5A, 5B). The reflectance spectrum is shown in Figure 5C. The pronounced absorption peak at 244 nm may be assigned to the optical plasma-resonance absorption of Rh-aggregates. Recently the optical properties of metallic Rh [12] and metallic-island Rh films [13] were studied. Features were observed at 1.1 eV (1128 nm), 2.68 eV (463 nm) and 5.8 eV (214 nm) in reflection spectra of the polycrystalline samples, which were interpreted as interband transitions [12]. The transmittance spectra of Rh island films with different particle diameters in the range of 55 – 280 nm exhibit bands at 2.15 eV (577 nm), 3.5 eV (355 nm) and 6.1 eV (203.5 nm). The dominant band at 3.5 eV (diameter ~ 280 nm) was assigned to the optical plasma-resonance absorption [13]. The position of UV-VIS bands for Rh island films and for Rh nanoparticle aggregates that formed at high temperature in air are surprisingly close, even though the surface of Rh aggregates is covered by rhodium oxide. It is worth noting that 38 nm diameter Pt and Pd particles are characterized by optical plasmon resonance absorptions [14] at the same wavelength as those of the plasmon band for Rh aggregates. The effective size of our Rh nanoparticle aggregates was estimated from the optical plasma - resonance absorption using the

dependence of optical plasma resonance on the size of Rh islands as determined by Anno [13] (Fig 6a). The absorption at 244 nm corresponds to an effective size of ~ 30 nm. This value is substantially higher than the 7.4 nm obtained by XRD measurements. In XRD, diffraction occurs on crystalline metallic nanoparticles and peaks become broader if there are fewer planes that give the rise to Bragg reflection. The increase in effective diameter from 5.5 to 7.4 nm may be interpreted as two Rh nanoparticles merging together (Figure 6b). The average size of Rh nanoparticles estimated from the location of the optical surface plasma- resonance [15a] reflects the size of electronically-connected clusters of metallic nanoparticles . This size is substantially higher than the size from X-ray scattering measurements, which give the size of the discrete Rh nanocrystals based on the coherence length of the atoms in the merged nanoparticles. The effect of nanoparticle aggregation on optical plasma-resonance position is due to organization of isometric metallic nanoparticles into arrays/clusters, which exhibit strong coupling to surface plasmons (red-shift of the SPR band) while leaving discreet metallic nanoparticles intact [15b].

Thermal Decomposition of PVP, Pt-PVP and Rh-PVP.

Conformational change of PVP. Decay in H_2, N_2 and O_2. The thermal stability of pure PVP has been extensively studied [16]. However, considerably less is known about the transformation of PVP capping agent on the surface of Rh and Pt nanocrystals subjected to high-temperature treatment under reducing and oxidizing conditions, a standard procedure in heterogeneous catalyst preparation. Monitoring the *in-situ* transformation of PVP, Rh-PVP, and Pt-PVP in the temperature range of 25-350 °C (heating rate 3.2°C/min) in N_2, H_2 and O_2 flow was done using a DRIFTS reactor. Assignments of

FTIR and Raman spectra were presented in a previous work [6]. The heating of PVP in H_2 and N_2 flow up to 200 °C did not substantially change the position of carbonyl band at 1680 cm^{-1}. Very small changes are seen in the region of CH stretching bands assigned to vibrations of the CH_2 groups in the chain and ring of PVP. As seen in Figure 7a, the band at 2873 cm^{-1} (assigned to tertiary C-H stretching vibrations) is more sensitive to the temperature changes. Substantial changes are also seen in bands at 1430 cm^{-1} (CH_2 scissors) and at 1280 cm^{-1} (CH_2 wag.) (Figure 7b). It should also be noted that the presence of isosbestic points in the spectra (Figure 7a, b) indicates the initial form of PVP converted into a new one quantitatively. This data shows that, up to 200 °C, PVP does not decompose in an H_2 atmosphere, but that the PVP chain structure and packing density changes, most likely due to a glass-transition and cross-linking [16]. Degradation of PVP in O_2 atmosphere starts at about 100 °C. The maximum of the carbonyl band shifts from 1680 cm^{-1} at 34 °C to 1720 cm^{-1} at 190 °C, a possible indication of the formation of aliphatic ketones [17]. The C-H stretching and bending modes of PVP simultaneously decrease in intensity above 100 °C, while two new bands and a doublet appear at 3325 cm^{-1}, 3075 cm^{-1}, and 2250-2223 cm^{-1} respectively.

Decay of capping PVP starts at the interface of PVP/Pt.

The decomposition of Pt-PVP and Rh-PVP nanoparticles was studied under similar experimental conditions. The spectra of PVP capping agent in N_2 and H_2 atmospheres gradually decrease in intensity above 200 °C. However, the various spectra for the initial Rh-PVP and its products in the temperature range of 30-200°C behave similarly, whereas in the case of Pt-PVP, new absorption bands appear near 2000 and 1810 cm^{-1} in the temperature range of 85-215 °C (Figure 7c). The appearance of the new bands

characteristic of linear and bridging carbon monoxide, indicates that pyrrolidone rings adsorbed on platinum atoms begin to decompose at ~100°C lower than the decomposition temperature for non-bonded amide groups as determined in present work by FTIR and by TGA [16]. It is interesting to note that Pt and Rh nanoparticles act as a trap for the carbon monoxide that is eliminated from side pyrrolidone rings adjacent to the metallic surface during degradation. In the H_2 atmosphere, loosely bonded PVP chains around Pt and Rh nanoparticles maintain their composition until 200 °C, in contrast to a thin layer of pyrrolidone rings adjacent to metal surface. The difference in thermal decomposition of the interfacial layer for Rh-PVP and Pt-PVP can be seen from a comparison of the intensity ratio for characteristic bands of amide carbonyls at 1680 cm^{-1} and C-H deformation modes at 1430 cm^{-1} and 1370 cm^{-1} for residual PVP (Figure 7c and 10c). The ratio of intensities C=O/C-H did not change in the case of Rh-PVP up to 220 °C; however the shape of C-H deformation modes change due to packing and cross-linking of the PVP capping agent. In the case of Pt-PVP, more noticeable features appear: the intensities of CH bands substantially decrease relative to the C=O carbonyl stretch and new carbon monoxide bands at 2020 cm^{-1} and a doublet centered at 1810 cm^{-1} appear in the temperature range of 80 -180 °C (Figure 7c).

Carbon monoxide adsorbed on Rh-PVP and Pt-PVP monitors the electronic state of metallic surface during PVP degradation.

Both the frequency and the intensity for the C≡O stretch of carbon monoxide adsorbed on Pt-PVP in a H_2 flow show (*in-situ* measurement) unusual maxima as functions of temperature. The frequencies for both linear and bridging carbon monoxides increase up to 160 °C, and decreases thereafter (Figure 8a). Under most circumstances, the frequency

of the carbon monoxide decreases if the surface of Pt nanoparticles is reduced in hydrogen at higher temperatures, since the ability of surface Pt atoms to contribute in $d\pi \rightarrow \pi^*$ back-bonding to adsorbed carbon monoxide is increased. It was previously shown that on the surface of Pt nanoparticles above 2 nm in size, only a monolayer of PtO, which is reducible by H_2 at 50-100 °C [11], was formed. Carbon monoxide adsorbed on Pt surfaces is a sensitive probe of two properties: the accessibility of platinum surface area and the electronic structure of the platinum surface [18]. The intensity of CO bands reflects the number of adsorbed CO molecules, while the CO frequency reflects the electron donating capabilities of the surface platinum atoms. The reduction of surface platinum atoms affects the interaction with adjacent pyrrolidone rings and chemisorbed carbon monoxide differently (Scheme 1). The reduction of Pt nanoparticles decreases charge-transfer interactions between carbonyl groups of pyrrolidone rings and platinum as followed using SERS [5], but increases the strength of CO chemisorption as a consequence of increased electron back-donation from Pt atoms to CO. We can only speculate on the reason for the maximum in the graph in Figure 8. The frequency of adsorbed carbon monoxide is a monitor of subtle changes in the electronic state of platinum atoms during thermal decay of capping agent in H_2 atmosphere. At low heating temperatures (80 – 160 °C), the donation of electron lone pairs from amide carbonyls bonded to $Pt^{\delta+}$ atoms decreases as surface platinum atoms in the reduced state repel the lone pair electrons of a carbonyl group, creating a new site on metallic nanoparticles for CO adsorption (Scheme 1). Above 160 °C, the reduction of the Pt surface plays a dominant role in lowering the CO stretch frequency. Shielding of the metal surface by products of the PVP thermal decomposition also takes place. We concluded, that the Pt

and Rh atoms on the surface of nanoparticles with ligated pyrrolidone rings and carbon monoxide behave similarly to coordination compounds [19].

CO adsorption on Rh-PVP and Pt-PVP after RedOx treatment.

The dependence of CO band intensity vs. reduction temperature of Pt-PVP and Rh-PVP in an excess of gas-phase carbon monoxide was studied. The samples were first subjected to reduction for 10 min in H_2 flow at temperatures ranging from 50 to 300 °C. Then the samples were pumped down to ~10^{-4} torr at room temperature and then repressurized with 260 ± 5 torr of CO and the FTIR spectrum measured. Thereafter oxygen was flowed at 30 °C over the sample to remove adsorbed carbon monoxide and this procedure was repeated with the same sample for treatments at 50, 100, 150, 200, 250 and 300 °C. It was found that about 25 min was necessary to reach saturation of the CO band intensity. Figure 9a shows that for Rh-PVP + CO, the shape of carbon monoxide bands transforms with time . Initially there are two CO bands, one at 2032 cm^{-1} (atop-linear structure) and the other at 1830 cm^{-1} (threefold hollow adsorption); after 5 min, a new band appears at 1880 cm^{-1} (bridge adsorption). For comparison, all spectra in Figure 9a were normalized to the absorbance of the 2032 cm^{-1} band. The simultaneous appearance of the two bands (2032 cm^{-1} and 1830 cm^{-1}) demonstrates that adsorption energies for atop sites and for hollow sites are very close and this is in good agreement with results of theoretical calculations of adsorption energies for CO on Rh(111) surfaces [20]. Increasing the temperature from 25 to 300 °C in H_2 flow resulted in decreasing both CO stretching frequency (Figure 9b) and integrated intensity (Figure 9c). The decrease of carbon monoxide frequency chemisorbed on the surface of nanoparticles is due to reduction of the surface of Rh and Pt particles, thereby increasing the $d\pi \rightarrow \pi^*$ back-

bonding to CO. The CO bands after treatment in H_2 above 300 °C can no longer be observed, suggesting that the residual products are occupying surface sites that are favorable for CO bonding. It should be noted that FTIR data for CO adsorption via *in-situ* measurements (Figure 7c, 8a and 8b) and in excess pressure of 'external' CO at room temperature (Figure 9) are distinctive and unclear. The first one monitors the *in-situ* transformation of the nanoparticle interface with Pt in highly reduced state with the CO frequencies ranging from 2020 to 1950 cm^{-1}. In RedOx mode the surface of Pt-PVP is more oxidized, as shown by the range of 2060-2040 cm^{-1} for the CO frequencies.

Polyamide-polyene products. Degradation of Pt-PVP and Rh-PVP in an oxygen atmosphere.

More complex changes of the PVP with increasing temperature were observed for neat PVP and Rh-PVP and Pt-PVP in O_2. While the intensities of all bands for Pt-PVP and Rh-PVP upon thermal decomposition gradually decreased, several new absorption bands of residual products appeared.

The data for Rh-PVP is summarized in Figure 10. Capping PVP is more stable in hydrogen than in oxygen (Fig. 10 a, b). In reducing conditions Rh-PVP loses carbonyl and CH groups starting at 220 °C and the ratio of integral intensities >C=O/CH increases (Figure 10 a, c). As can see in Figure 10c, the spectra of initial product at 30 °C and those of the residual at 220 °C are very close, which means that the capping PVP (55 K, MW) releases low molecular weight fragments. Noticeable decomposition of capping PVP in oxygen starts at 170 °C and ratio >C=O/CH has a maxima near 260 °C, which reflects appearance new of oxygenates with carbonyl bands at 1718 and1780 cm^{-1} (Fig. 10 b, d). The decrease of the aliphatic CH band intensity relative to that of the >C=O band of the

pyrrolidone rings demonstrates that during heating of Rh-PVP, the aliphatic units of the backbone undergo thermal degradation, probably due to dehydrogenation (Scheme 2).

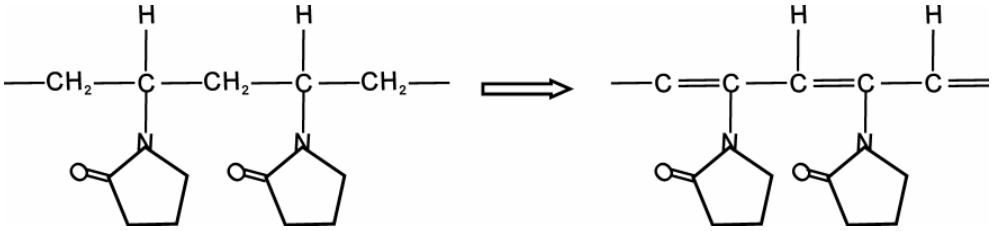

Scheme 2

Additional evidence in favor backbone dehydrogenation may be seen in the spectra of Rh-PVP at temperatures above 180 °C (Figure 11). An absorbance at 1590-1610 cm^{-1} appears and shifts to lower frequencies with increasing temperature. This band may be assigned to the C=C stretch of polyene sequences [17] (Figure 11 a, b). The band at 1610 cm^{-1} also appeared in oxidizing environments for pure PVP, Rh-PVP, and Pt-PVP, but at different temperatures. In Fig. 11c one can see the appearance new bands at 3340, 3080, 2230, 2157 and 1590 cm^{-1} at high temperature. IR peak assignments is presented in Table 2 for residual products formed at 280 °C (ramp 3.2 °C /min) from pure PVP and Rh-PVP in O_2 flow. As seen in Fig. 11 and Table 2, during the thermal decay of pure PVP and of PVP capped Rh nanoparticles, new compounds form with N-H bonds (3330-3342 cm^{-1}), nitrile bonds (2161-2254 cm^{-1}), polyene >C=C< groups (3089 and 1600 cm^{-1}, Figure 12a-b), and possibly aldehyde groups (1703-1735 and 1335 cm^{-1}). The positions of these adsorption bands are slightly shifted on Rh-PVP/Al compared to PVP/Al and new peaks appear in case of Rh-PVP as well.

TABLE 2

PVP in O_2	**Rh-PVP in O_2**	**Assignment**
3330	3342	N—H
3082	3089	C—H, vinyl
	2968	C-H, ν_{as} (CH_3)
2940	2937	C—H, ν_{as}(CH_2)
2254	2246	ν(C≡N)
2226	2222	ν(C≡N)
	2161	ν(C≡N)
1780	1780	>C=O or C≡N
1735-1724	1718-1703	ν(>C=O), amide I
1600	1595	ν(C=C—C=C) ν(arom. ring, amide II)
1328	1335	δ(CH), -CHO,
	1158	ν(C—C), CCHO

It is believed that the differences between the spectra of pure PVP and those of Rh-PVP residual products originates from active oxygen attack (O_2 spill-over from Rh surface) of Rh-PVP, and from the fact that drop-casted layers of Rh-PVP after high-temperature treatment in O_2, transform into a thin layer of residual products bonded to the surface of rhodium nanoparticles. The residual products of deposited on Al-foil PVP degradation

bond to the surface of Al_2O_3. The FTIR spectra of the residuals also reveal some absorption bands similar to those that appear in the spectra of residual non-volatile char formed during the process of thermal degradation of polyamide [21]. PVP is an addition polymer that has aliphatic hydrogen atoms along the backbone that are easily transferred following homolytic bonds cleavage in the temperature range of 200°C -300°C [22]. One may speculate that above 250°C, capping PVP transforms into a polyamide-polyene structure.

We measured the deep UV-Raman spectrum of the non-volatile char that formed from Rh-PVP and Pt-PVP deposited on Al-foil after oxidation in O_2 and after reduction in H_2 (heating to 300 °C, 3.2 °C/min). It was found that in the Raman spectra of both chars (Rh and Pt nanoparticles) intense and broad peaks appear at ~1595 cm^{-1} and ~1380 cm^{-1} (Figure 12c), indicative of the presence of disordered graphite . These two peaks may be assigned to the G and D vibrations (so-called carbon sp^2-type) of disordered amorphous carbon [23]. The weak peak at 1030 (cm^{-1}) (T) may be a trace of sp^3-type tetrahedral amorphous carbon. Recently we have shown by deep UV-Raman that Pt-PVP thermally degrades in the air at 350 °C to amorphous carbon [6].

Thus the heating of PVP stabilizer capped Rh nanoparticles occurs in a number of steps: conformational change of the PVP, production of polyene sequences with polyamide-polyene fragments and several end-groups such as –C≡N and CHO, and finally the formation of char, which is made up of amorphous carbon. At temperatures above 250 °C in O_2, a thin layer of a complex composite material forms on the surface of Rh and Pt nanoparticles, comprised of polyamide - polyene fragments and amorphous carbon (Figure 12d).

CONCLUSIONS

We have shown that spectroscopic techniques are very effective tool to study the degradation of poly(N-vinylpyrrolidone) stabilizer of rhodium and platinum nanoparticles, the electronic structure of the metal/PVP interface and the aggregation of nanoparticles. The spectroscopic study of the thermal decay of PVP stabilizer in H_2 and O_2 atmospheres shows the formation of 'polyamid-polyene' like material (above 250 °C), which then transforms into amorphous carbon (above 300 °C). The behavior of low-coordinated surface Rh and Pt atoms with ligated CO and amid groups of PVP resembles that of 'surface coordinated compounds'.

ACKNOWLEDGMENT

We are truly grateful to Prof. Herbert L. Strauss for his valuable advice during preparation of this paper. This work was supported by the Director, Office of Science, Office of
Basic Energy Sciences, Division of Chemical Sciences, Geological and
Biosciences and Division of Materials Sciences and Engineering of the
U.S. Department of Energy under contract No. DE-AC02-05CH11231.

References

1 Fievet, F.; Lagier, J. P.; Blin, B.; Beaudoin, M.; Figlarz, M. *Solid State Ionics* **1989**, *32/33*, 198; Viau, G.; Fievet-Vincent, F; Fievet, F. *Solid State Ionics* **1996**, *84*, 259; Song, H.; Kim, F.; Connor, S.; Somorjai, G. A.; Yang, P. *J. Phys. Chem. B.* **2005**, *109*, 188; Wiley, B.; Sun, Y.; Mayers, B.; Xia, Y. *Chem. Eur. J.* **2005**, *11*, 454.

2 Didier Astruc, Ed. *Nanoparticles and Catalysis*, **2007**, Wiley-VCH, Weinheim; Song, H; Rioux, R.M.; Hoefelmeyer, J.D.; Komor, R.; Niez, K.; Grass, M.; Yang, P.D.; Somorjai G.A. *J. Am. Chem. Soc*. **2006**, 128, 3027; Bratlie, K.M.; Klliewer, C.J.; Somorjai G.A. *J. Phys. Chem. B*, **2006**, 110, 17925; Somorjai, G.A. and Park, J.Y. *Angew. Chem. Int. Ed*. **2008**, 47/48, 9212

a) Aliaga, C.; Park,J.Y.; Yamada, Y.; Lee, H.S.; Tsung, C.K.; Yang, P.D.; Somorjai, G.A. *J. Phys. Chem. C,* **2009**, 113/15, 6150.

3 Zhang, Y; Grass, E.G.; Habas, S.E.; Tao, F; Zhang, T; Yang, P.; Somorjai,G.A. *J. Phys*. *Chem. C*. **2007**, 111, 12243.

4 Borodko, Y.; Ager, J.W.; Marti, G.E.; Song, H.; Niesz, K. and Somorjai, G.A. *J. Phys*. *Chem. B* **2005**, 109, 17386.

5 Borodko, Y.; Humphrey, S.M.; Tilley, T.D.; Frei, H. and Somorjai, G.A. *J. Phys*. *Chem. C*. **2007**, 111, 6288.

6 Borodko, Y.; Habas, S.E.; Koebel, M.; Yang, P.; Frei, H. and Somorjai, G.A. *J. Phys. Chem. B* **2006**, 110, 23052

7 Zettsu, N.; McLellan, J.M.; Wiley, B.; Yin, Y.; Li, Z.-Y. and Xia, Y. *Angew. Chem. Int. Ed.* **2006**, 45, 1288. Zhang, Y.; Grass, M.E.; Habas, S.E.; Tao,F.; Zhang, T.; Yang, P. and Somorjai, G.A. *J. Phys. Chem. C* **2007**, 111, 12243. Humphrey, S.M.;

Grass, M.E.; Habas, S.E.; Niez, K.; Somorjai, G.A. and Tilley, T.D. *Nano Letters* **2007**, 7/3, 785

8 Bohren, C.F.; Huffman, D.R. *Absorption and Scattering of Light by Small Particles. Wiley-VCH, Weinheim*, **2004**.

9 Harrick, N.J. *Applied Optics* **1971**, 10/10, 2344. Hind, A.R. and Chomette, L. The determination of thin film thickness using reflectance spectroscopy. *Varian UV at Work No. 090, www.varianinc.com.* Guan, Y.; Yang, S.; Zhang, Y., Xu, J., Han, C.C.; Kotov, N.A. *J. Phys. Chem. B* **2006**,110/27, 13484. Williams, C.T.; Chen, E.K.-Y. ; Takoudis, C.G. and Weaver, M.J. *J. Phys. Chem. B* **1998**, 102, 4785.

10 Grass, M.E.; Zhang, Y.; Butcher, D.R.; Park,J.Y.; Li,Y.; Bluhm, H.; Bratlie K.M.; Zhang, T. and Somorjai, G.A. *Angew. Chem. Int. Ed.* **2008**, 47, 8893. Munoz, A.*;* Munuera, G.; Malet, P.; Gonzalez-Elipe, A.R. and Espinos, J.P. *Surf. and Interface Analysis* **1988**, 12, 247.

11 McCabe, R.W.; Wong, C.; Woo, H.S. *J. Catal.* **1988**, 114, 354. Huzinga, T.; Van Grondelle, J.; Prins, R. *Appl. Catal. **1984**, 10, 199.*

12 Weaver, J.H. *Physical Review B* **1975**, 11/4, 1416. Weaver, J.H.; Olson, C.G.; Lynch,D.W. *Phyical. Review B* **1977**, 15/8, 4115. Pierce, D.T. and Spicer, W.E. *Phys. Stat. Sol. (b)* **1973**, 60, 689.

13 Anno, E. *Physical Review* B **1996**, 53/7, 4170. Anno, E.; Tanimoto, M. *J. Appl. Phys.,* **2000**, 88/6, 3426.

14 Langhammer, C.; Yuan, Z.; Zoric, I. and Kasemo, B. *Nano Letters*, **2006**, 6/4, 833.

15 a) Kreibig, U. and Fragstein, C. Z. Phys. **1969**, 224, 307; b) Lin,S.; Li, M.; Dujardin, E.; Girard, C.; Mann, S. Adv. Mater. **2005**, 15, 2553

16 Yoshida, M. and Prasad, P.N. *Appl. Optics* **1996**, 35/9, 1500. Scheirs, J.; Bigger, S.W.;Then, E.T.H.; Billingham, N.C. *J. Polym. Sci. B: Polymer Physics*, **1993**, 31, 287. Peniche, C.; Zaldivar, D.; Pazos, M.; Paz, S.; Bulay, A.; Roman, J.S *J. Appl. Polym. Sci.,* **1993**, 50, 485. Du, Y.K.; Yang,P.; Mou, Z.G.; Hua, N.P.; Jiang, L. *J. Appl. Polymer Science* **2006**, 99, 23.

17 Colthup, N.B.; Daly, L.H.; Wiberley, S.E. *Introduction to Infrared and Raman Spectroscopy,* Acad. Press, **1990** San Diego.

18 Thomas, J.M. and Thomas W.J. *Introduction to the Principles of Heterogeneous Catalysis*, Academic, London, **1967.** Knozinger, H, in: Ertl, G.; Knozinger, H.; Weitkamp, J. (Eds.), *Handbook of Heterogeneous Catalysis,* vol. 2, Wiley-VCH, Weinheim, **1997**, p. 707. Davydov, A. *Molecular Spectroscopy of Oxide Catalyst Surfaces*, Willey, Chichester, **2003**.

19 Hemminger, J.C.; Muetterties, E.L. and Somorjai, G.A. *J. Am. Chem. Soc*. **1979**, 101, 62. Barth, J.V. *Surf. Science*, in press **2009** doi:10,1016/j.susc.2008.09.049

20 Mason, S.E.; Grinberg, I. and Rappe, M. *Phys. Rev. B,* **2004**, 69, 161401 (R); Abild-Pedersen, F.; Andersson, M.P. Surf. Sci., **2007**, 601, 1747.

21 Holland, B.J.; Hay, J.N. *Polym. Int*. **2000**, 49, 943. Nyden, M.R. *Appl. Spectr*. **1999**, 53, 1653.

22 Montaudo, G.,Puglisi, C. in Development in Polymer Degradation. Grassie, N. Ed. *Appl. Sci.* 1987, 7, London; in Comprehensive Polymer Sci. First Suppl. Pergamon Press, Oxford, 1992, p. 227.

23 Ferrari, A.C.; Robertson, J. *Phys. Rev.* B **2001**, 64/7, 75414; *Phil. Trans. R. Soc. Lond.* A **2004**, 362/1824, 2477. Hoffmann, G.G.; de With, G.; Loos, J. *Macromol. Symp.* **2008**, 265, 1-11

FUGURE CAPTIONS

Figure 1. TEM analysis of PVP stabilized Pt nanoparticles (a) and Rh nanoparticles (b).

Figure 2. UV-VIS spectra: A) Absorbance of pure PVP layers (1.3μ, 3.8μ and 4.2μ) deposited on quartz window; B) Comparison of UV-VIS spectra of Rh-PVP: absorbance in ethanol solution (a), absorbance of dry layer on quartz window (b) and absorptance (reflection mode) layer deposited on Al-foil (B, c). C) Effect of Rh-PVP layer thickness (1.3μ d; 3.8μ e; and 4.2μ f) on the ratio of intensities: PVP ($n \rightarrow \pi^*$) charge-transfer bands Rh ← O=C< ; D) Absorbance spectra of Rh-PVP for 3μ layer (1) and 5μ layer (2) (transmission mode). In insert (D, 1a): interference fringe pattern for 3μ layer.

Figure 3. Scheme of possible types for absorption bands Pt- and Rh-PVP in UV-VIS region. A) Effect of reduction in H_2 on CT bands Pt-PVP and Rh-PVP (*in-situ*) and B) effect of Rh-PVP oxidation on absorptance spectra (temperature range 30 -550 °C, *ex-situ*).

Figure 4. The SEM and XRD data for Rh-PVP (A) and Pt-PVP (B) heated in air.

Figure 5 The scheme of reflectance measurements: A) with reflecting media behind the sample, and reference; B) without reflectors behind the sample and reference. C) Reflectance spectra of Rh-PVP after heating layer of Rh-PVP deposited on quartz at 550°C and 350 °C (Scheme B).

Figure 6. a) Evaluation of the Rh aggregates size after heating in air Rh-PVP nanoparticles (7 nm) based on optical plasmon-resonance location taken from the work of Anno [13] and b) comparison effective size of Rh aggregates with surface plasma-resonance (SPR) at 240 nm with XRD measurements.

Figure 7. Temperature dependence of FTIR-DRIFT spectra of PVP in H_2 flow. The heating only slightly affect the CH stretching bands (a), however CH_2 deformation modes: scissors (1430 cm^{-1}) and wagging (1300 cm^{-1}) are more sensitive to the temperature increase (b). c) FTIR *in-situ* spectra of Pt-PVP heated in flowing H_2. During degradation, elimination of CO from side pyrrolidone rings may occur. Carbon monoxide adsorbed on Pt nanoparticles appeared in the temperature range of 100–200 °C.

Figure 8. The effect of heating Pt-PVP nanoparticles in H_2: on the adsorbed carbon monoxide frequencies: a) linear atop (n) and bridging (△) structures; and on the intensities of these bands (b) and carbonyl band of capping PVP (◗)

Figure 9. a) The change of relative intensities of the three CO bands: 2032 cm^{-1} (atop structure), 1880 cm^{-1} (bridging structure) and 1830 cm^{-1} (threefold hollow structure) with time for (Rh-PVP) + CO. The CO stretch absorbance for atop structure was used to normalize intensities. b) The effect of heating Pt-PVP in hydrogen on CO bands position (■- linear atop structure; □-bridging structure) and (c) CO bands intensities.

Figure 10. FTIR spectra of Rh-PVP in H_2 and O_2 media. a) The ratio of integral intensities >C=O/CH during heating in H_2 (3.2 °C /min); b) The ratio of integral intensities >C=O/CH during heating in O_2 (3.2 °C /min); c, d) The

overview *in-situ* spectra of Rh-PVP in the range 1000-3500 cm^{-1} and temperature range 35-250 °C in H_2 (c) and O_2 (d).

Figure 11. Effect of heating Rh-PVP nanoparticles in O_2 flow on FTIR-DRIFT spectra in the temperature range 30 - 300°C. a) Overview FTIR spectra of Rh-PVP in the spectral range 3600– 850 cm^{-1}. b) Appearance at high temperature a new bands at 1775, 1714 (>C=O) and at 1610 cm^{-1} (>C=C<). c) Comparison the initial spectrum of Rh-PVP at 50 °C (black line) with spectrum of residual at 285 °C (grey line). Both spectra were normalized to the carbonyl absorption. The residual has new bands at 3340 (N-H), 3080, 1590 (H-C=C<), 2230 and 2157 cm^{-1} (-C≡N), which are characteristic of 'polyamid-polyene' like structure.

Figure 12. a, b) Appearance and gradual increase intensity of band at 1610 cm^{-1} (carbon-carbon double bond) and absorbance above 1700 cm^{-1} (new carbonyl bonds). c) Raman spectrum of residual after heating Rh-PVP at 350 °C in H_2. d) The cartoon shows the intermediate formation of residual product with dehydrated backbone and some end groups.

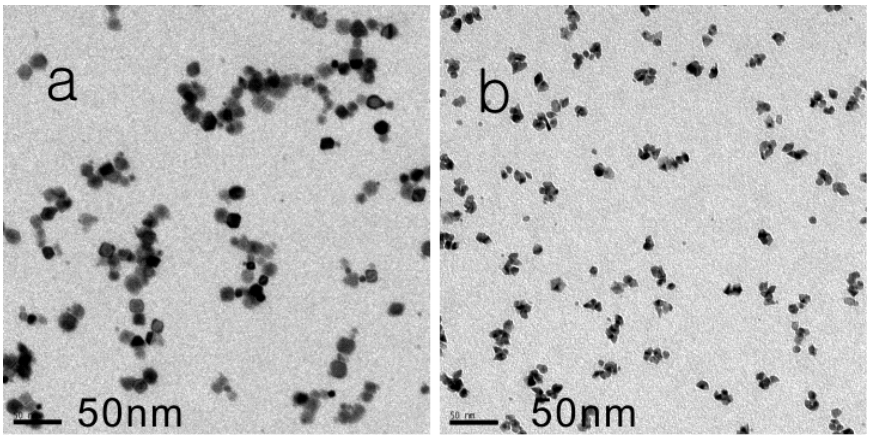

Figure 1.

TEM analysis of PVP stabilized Pt nanoparticles (a) and Rh nanoparticles (b).

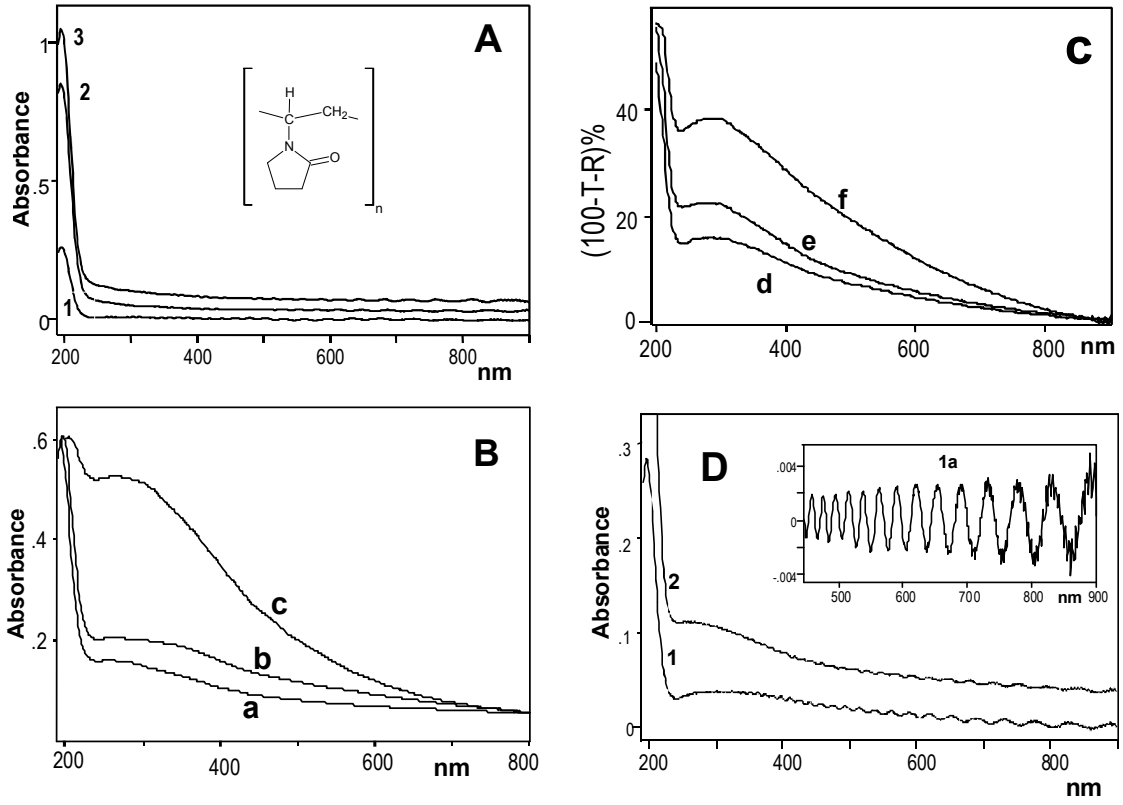

Figure 2. UV-VIS spectra: A) Absorbance of pure PVP layers (1.3μ, 3.8μ and 4.2μ) deposited on quartz window; B) Comparison of UV-VIS spectra of Rh-PVP: absorbance in ethanol solution (a); absorbance of dry layer on quartz window (b) and absorptance (reflection mode) layer deposited on Al-foil (B, c). C) Effect of Rh-PVP layer thickness (1.3μ, d; 3.8μ, e; and 4.2μ, f) on the ratio of intensities: PVP ($n \rightarrow \pi^*$) charge-transfer bands Rh ← O=C< ; D) Absorbance spectra of Rh-PVP for 3μ layer (1) and 5μ layer (2) (transmission mode). In insert (D, 1a): interference fringe pattern for 3μ layer.

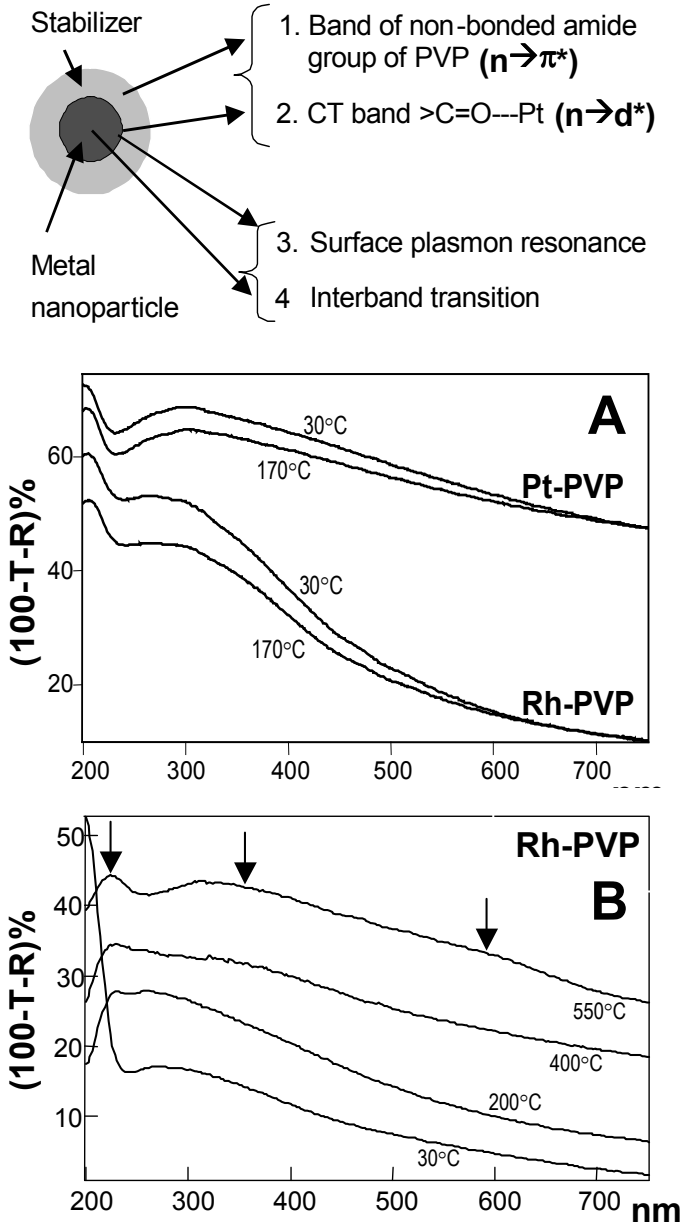

Figure 3 Scheme of possible types for absorption bands Pt- and Rh-PVP in UV-VIS region (top). (A) Effect of reduction in H_2 on CT bands Pt-PVP and Rh-PVP (*in-situ*) and (B) effect of Rh-PVP oxidation on absorptance spectra (temperature range 30 -550 °C, *ex-situ* measurement).

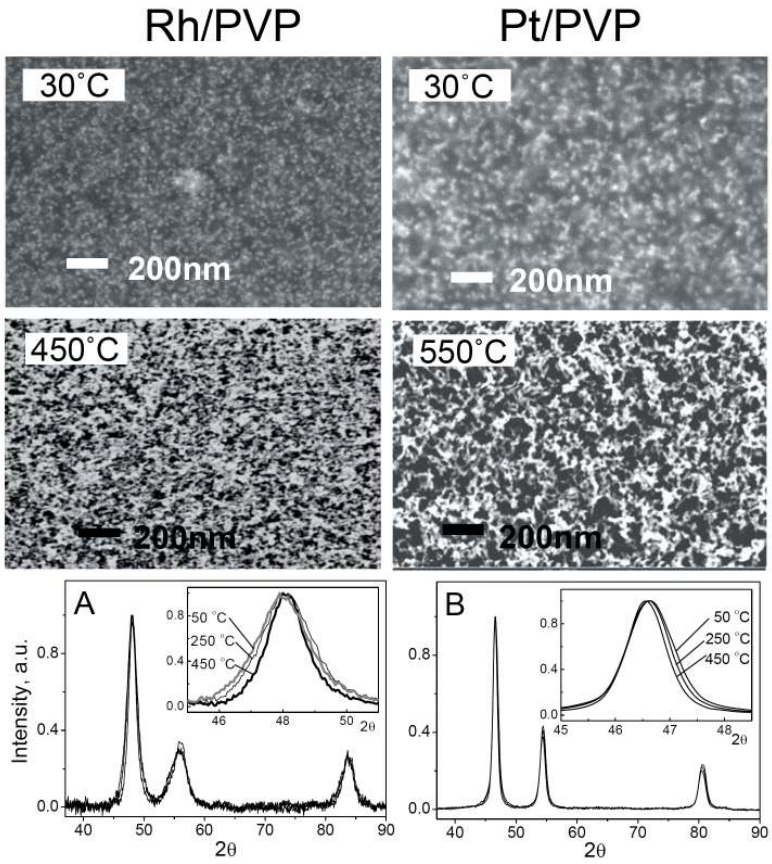

Figure 4 The SEM and XRD data for Rh-PVP (A) and Pt-PVP (B) heated in air.

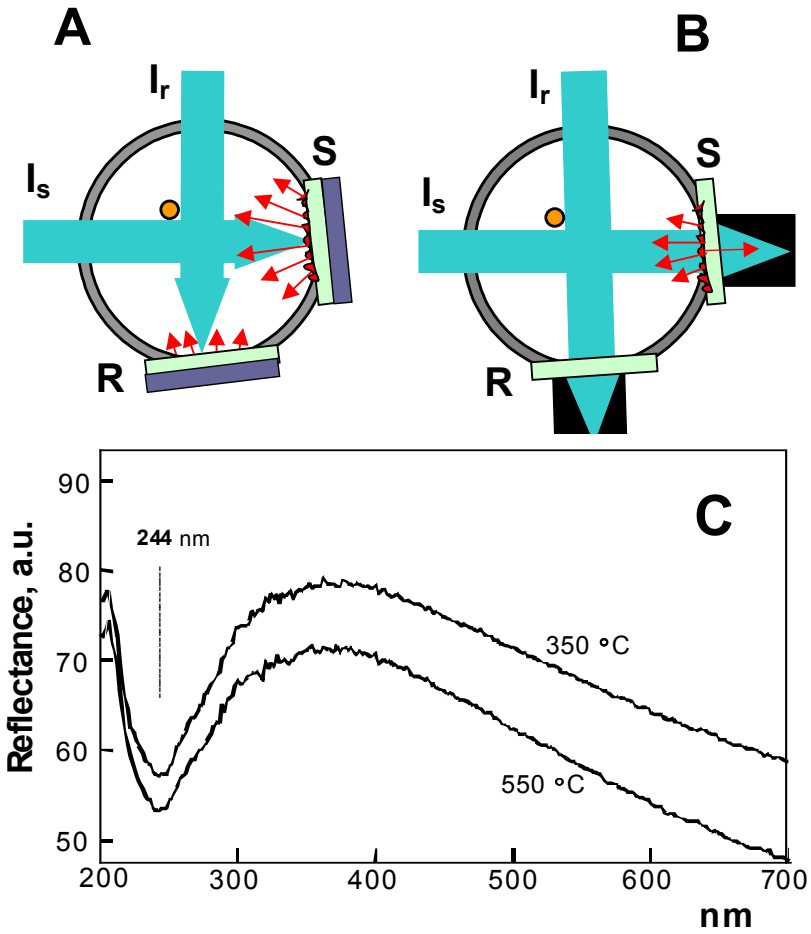

Figure 5 The scheme of reflectance measurements: A) with reflecting media behind the sample, and reference; B) without reflectors behind the sample and reference. C) Reflectance spectra of Rh-PVP after heating layer of Rh-PVP deposited on quartz at 550 °C and 350 °C in air (Scheme B).

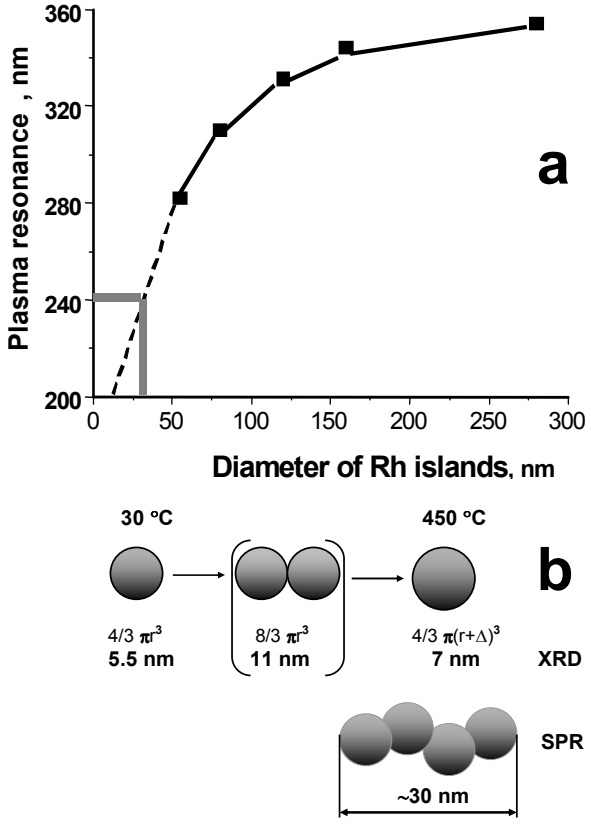

Figure 6 a) Evaluation of the Rh aggregates size after heating in air Rh-PVP nanoparticles (7 nm) based on optical plasma-resonance location taken from the work of Anno [13] and b) comparison effective size of Rh-clusters with surface plasma-resonance at 240 nm with XRD measurements.

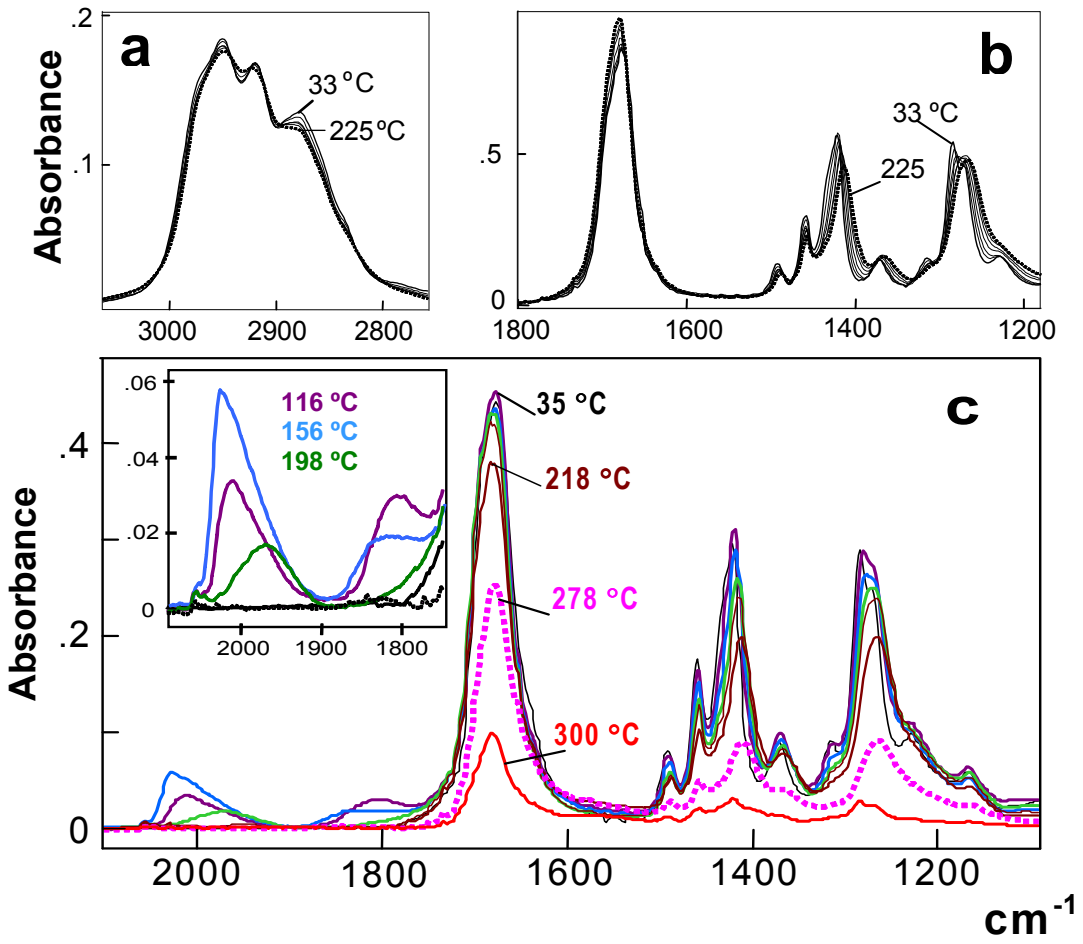

Figure 7. Temperature dependence of FTIR-DRIFT spectra of PVP in H_2 flow. a) The heating only slightly affect the CH stretching bands, however CH_2 deformation modes: scissors (1430 cm^{-1}) and wagging (1300 cm^{-1}) are more sensitive to the temperature increase (b). c) FTIR *in-situ* spectra of Pt-PVP heated in flowing H_2. During degradation, elimination of CO from side pyrrolidone rings occurs. Carbon monoxide adsorbed on Pt nanoparticles appeared in the temperature range of 100 °C – 200 °C.

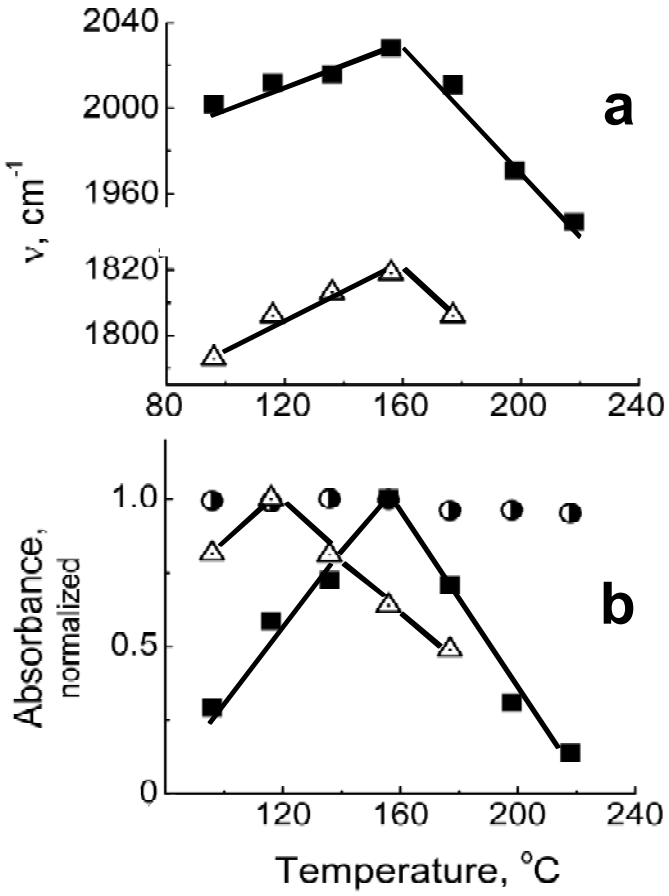

Figure 8. The effect of heating Pt-PVP nanoparticles in H_2. a) On the adsorbed carbon monoxide frequency: linear atop (n) and bridging (△) structures, and on the intensities of these bands and carbonyl band >C=O of capping PVP (◗).

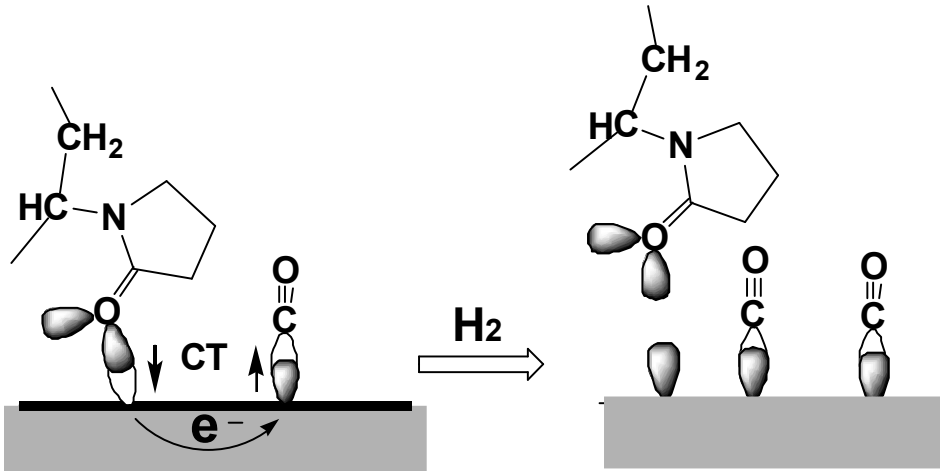

Scheme 1

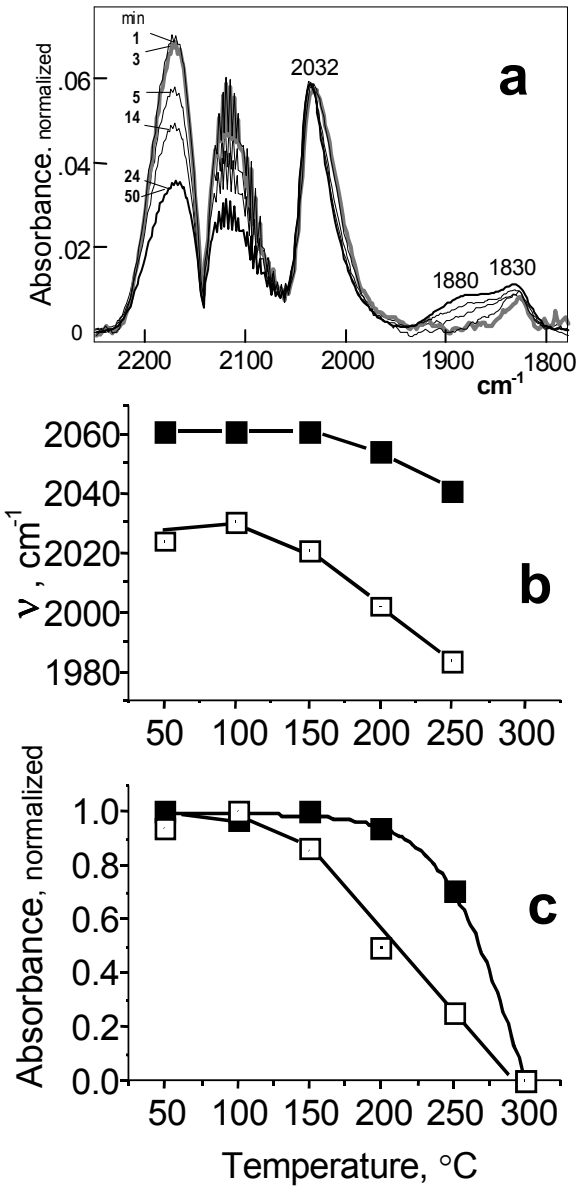

Figure 9.

a) The change of relative intensities of the three CO bands: 2032 cm^{-1} (atop structure), 1880 cm^{-1} (bridging structure) and 1830 cm^{-1} (threefold hollow structure) with time for Rh-PVP + CO. The CO stretch absorbance for atop structure was used to normalize intensities. b) The effect of heating Pt-PVP in hydrogen on CO bands position (■- linear atop structure; □-bridging structure) and CO bands intensities (c).

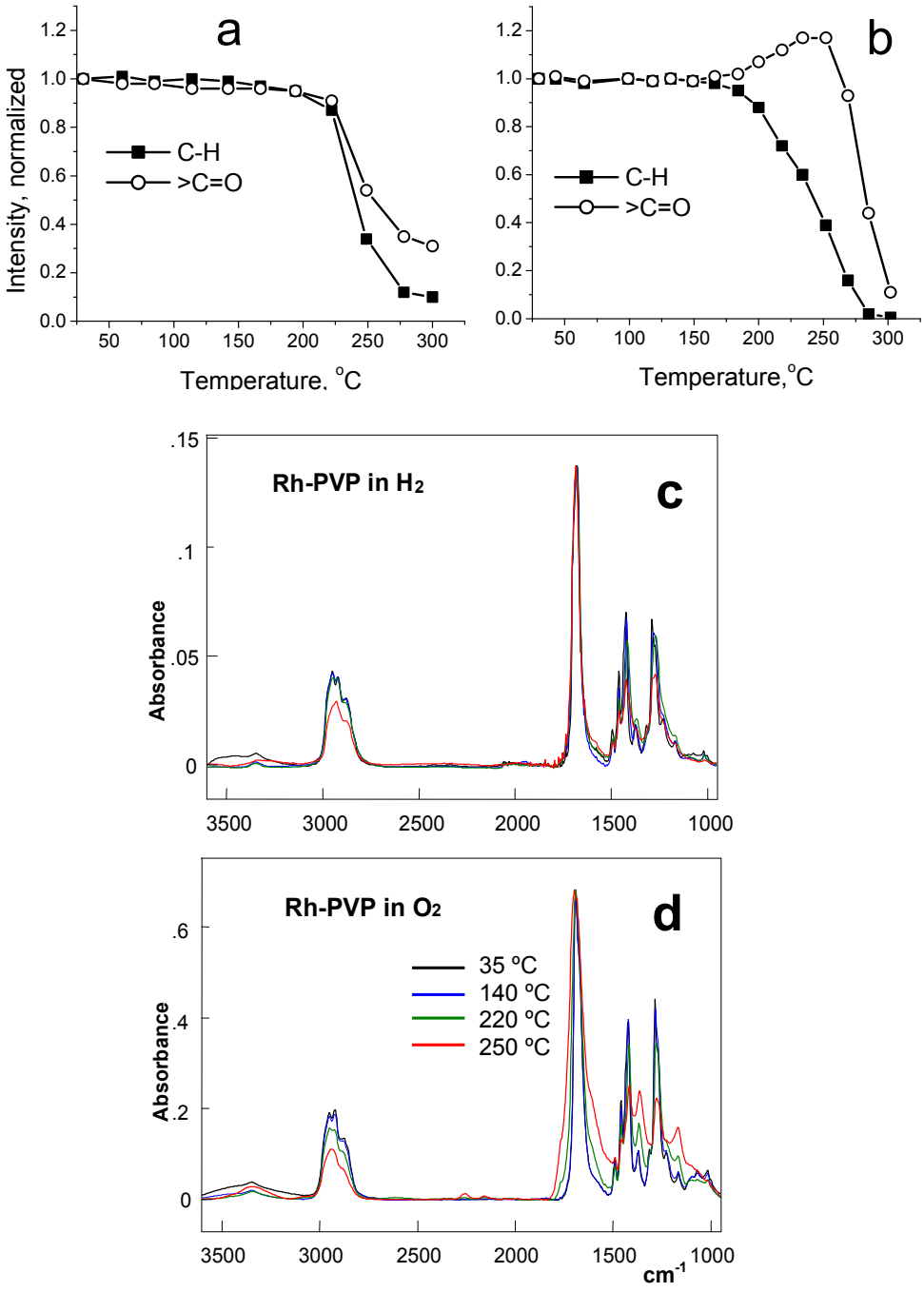

Figure 10. FTIR spectra of Rh-PVP in H_2 and O_2 media. a) Normalized integral intensities of >C=O and CH. Heating in H_2 (3.2 °C /min); b) Normalized integral intensities >C=O and CH during heating in O_2 (3.2 °C /min); The overview *in-situ* FTIR spectra of Rh-PVP in the range 1000-3500 cm^{-1} and temperature range 35-250 °C in H_2 (c) and O_2 (d).

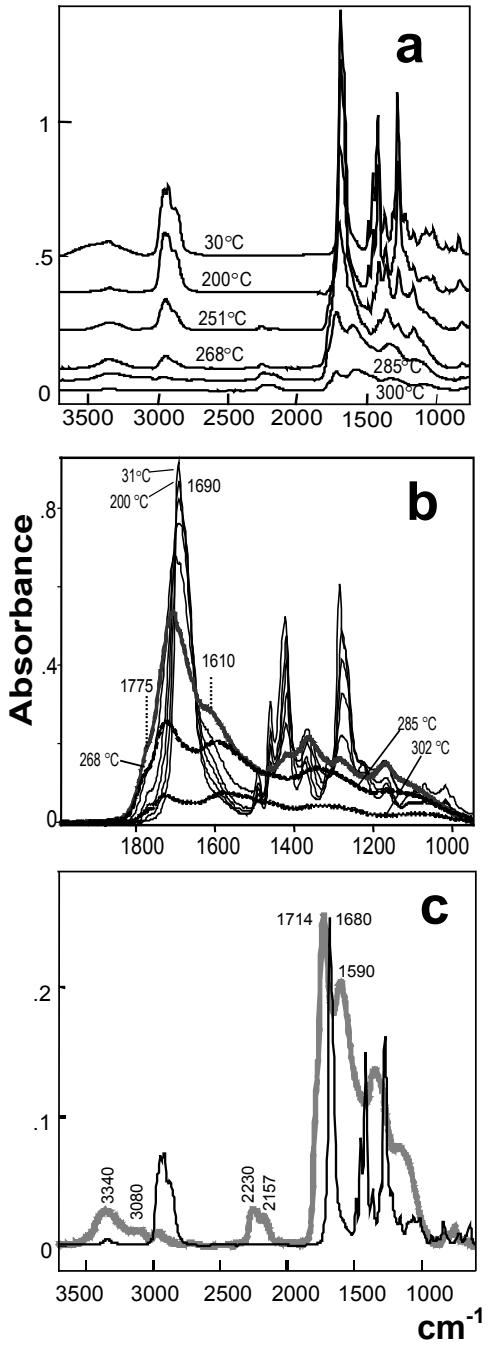

Figure 11.

Effect of heating Rh-PVP nanoparticles in O_2 flow on FTIR-DRIFT spectra in the temperature range 30 - 300°C. a) Overview FTIR spectra of Rh-PVP in the spectral range 3600– 850 cm^{-1}.
b) Appearance at high temperature a new bands at 1775, 1714 (>C=O) and at 1610 cm^{-1} (>C=C<).
c) Comparison the initial spectrum of Rh-PVP at 50 °C (black line) with spectrum of residual at 285 °C (grey line). Both spectra were normalized to the carbonyl absorbance. The residual has new bands at 3340 (N-H), 3080, 1590 (H-C=C<), 2230 and 2157 cm^{-1} (-C≡N), which are characteristic of 'polyamid-polyene' like structure.

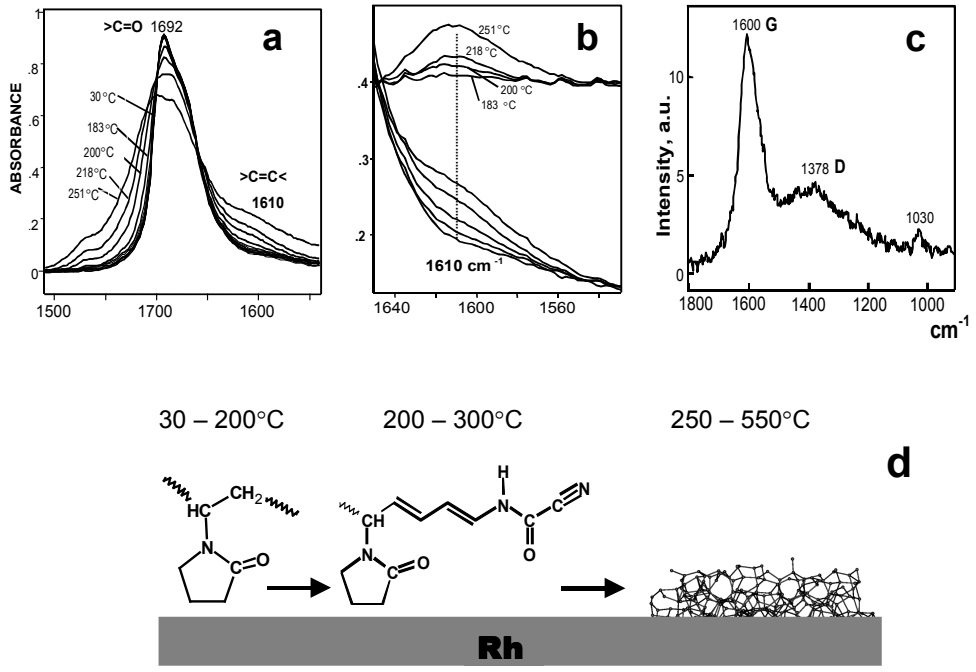

Figure 12.

a, b) Appearance and gradual increase intensity of band at 1610 cm^{-1} (carbon-carbon double bond) and absorbance above 1700 cm^{-1} (new carbonyl bonds). c) UV-Raman spectrum of residual after heating Rh-PVP at 350 °C in H_2. d) Cartoon shows the intermediate formation of residual product with dehydrated backbone and new end groups.

Table of Contents (TOF) Image.

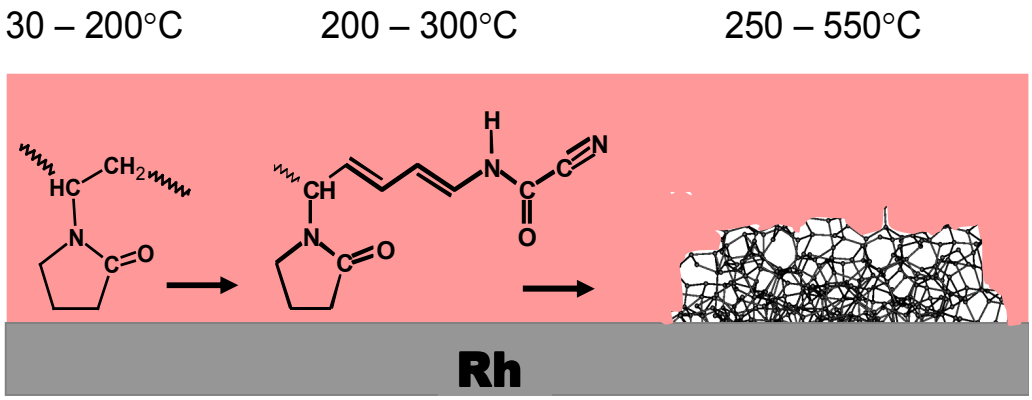

LEGAL DISCLAIMER